J. Appl. Comput. Mech., xx(x) (2025) 1-13
DOI: 10.22055/jacm.2025.48646.5391

ISSN: 2383-4536
jacm.scu.ac.ir

Shahid Chamran University of Ahvaz

Journal of Applied and Computational Mechanics

Research Paper

Mathematical Modeling and Sensitivity Analysis of Enzymatic Biofuel Cells with Various Electrode Geometries

Regunathan Rajalakshmi[1], Annamalai Marimuthu[2], Sethu Naganathan[3], Lakshmanan Rajendran[2], Mohammad Izadi[4]

[1] Department of Mathematics, Alagappa University, Government Arts College for Women, Ramanathapuram-623501, India, Email: rajiharini2010@gmail.com
[2] Department of Mathematics, AMET University, Chennai-603112, India, Email: marimuthu250274@gmail.com (A.M.); Dr.Rajendran.L@gmail.com (L.R.)
[3] Department of Mathematics, Sethupathy Government Arts College, Ramanathapuram-623502, India, Email: nathanaga@gmail.com
[4] Department of Applied Mathematics, Faculty of Mathematics and Computer, Shahid Bahonar University, Kerman 76169-14111, Iran, Email: izadi@uk.ac.ir

Received July 28 2025; Revised October 19 2025; Accepted for publication October 31 2025.
✉ Corresponding authors: L. Rajendran (Dr.Rajendran.L@gmail.com), M. Izadi (izadi@uk.ac.ir)

Abstract. The mathematical model in this study advances prior research on enzymatic biofuel cells by applying the Rajendran–Joy method, which enables approximate analytical solutions of nonlinear reaction–diffusion equations incorporating Michaelis–Menten-type enzyme kinetics. Unlike many earlier models that primarily relied on numerical simulation or simplified linear assumptions, this study provides explicit analytical expressions for substrate concentration profiles and current–potential relationships for multiple electrode geometries (planar, cylindrical, spherical). The analytical approach delivers high accuracy validated against numerical simulations, allowing systematic parametric sensitivity analysis to reveal how critical parameters—such as the Thiele modulus, Michaelis–Menten constants for substrate and mediator, applied potential, and electrode geometry—govern biofuel cell performance. This enhances mechanistic understanding and design optimization, including evaluation of limiting cases, thereby offering new insights beyond previous methods that were either purely numerical or less comprehensive in addressing nonlinear kinetics and geometric effects.

Keywords: Mathematical modelling, Nonlinear equations, Biofuel cell, Analytical and numerical method, Reaction-diffusion equation, Sensitivity Analysis.

1. Introduction

There is a significant interest in the development of biofuel cell due to their ability to generate non-hazardous and environmentally benign energy to tackle the future global energy demand [1, 2]. Extensive research has been conducted on biofuel cells (BFCs) due to the possibility of miniaturization and thereby fit into portable electronic devices. These cells have been used in robotics, aerospace, transportation, and telecommunication [3, 4]. In recent years, enzymatic biofuel cells have attracted considerable interest owing to their simplicity and the availability of redox enzymes that can be readily extracted and purified from biological systems [5]. Enzymatic biofuel cells convert the chemically generated energy of biofuels into electrical power via the use of enzymatic processes as catalysts. There has been a lot of interest in their potential to replace conventional energy sources. Enzyme-modified electrodes are utilized in electrochemical detectors, bioreactors, medicinal implants, and biological chemistry to gain insights into enzyme functionality. Conventional electrochemical techniques such as cyclic voltammetry and chronoamperometry are commonly used to study enzymatic biofuel cells and electrodes [6, 7].

Mediated bioelectrocatalysis is highly helpful in constructing biosensors, bioreactors, and biofuel cells [8]. Tamaki et al. [9, 10] developed a biofuel cell electrode using surface-modified carbon to generate a substantial current density. Barton et al. [11] realized a high current density using a carbon-cloth composite electrode. Davis et al. show that the most recent advances in biofuel cells use catalytic enzymes to convert chemical fuels into electrical power [12]. Gu et al. [13–15] and Song et al. [6] improved biofuel cell performance and self-powered biosensing using conjugated organic nanozymes and nanomaterial-based hybrids, enhancing power density, sensitivity, and autonomous operation for real time biomedical monitoring of exosomes and microRNAs.

Solutions of reaction-diffusion equations in enzyme electrodes have been obtained analytically [17-19] and numerically [20, 21] under inadequate limiting conditions. Wen et al. [22, 23] engineered carbon fibre-carbon nanotube electrodes for glucose oxidase immobilization, enhancing electron transfer and bioanode efficiency in biofuel cells. Modelling and simulation are essential tools to better understand and improve biofuel cell performance [24, 25]. Validated models should be employed to analyze reactions, design new electrodes, and accelerate practical system development alongside experimental studies. However, only a few models

Published online: November 05 2025

have been developed to date. These models have a few essential exclusions, such as flow of fluids, transfer of heat, ion migration, interactions, and spatial variations [26, 27].

Sensitivity analysis in EBFCs helps clarify the impact of kinetic parameters on system performance and supports optimization. De Oliveira et al. [28] developed a kinetic model showing key parameters influencing current in ethanol fuel cells, while Padierna-Vanegas et al. [29] highlighted parameter identifiability using dynamic modeling to improve predictive accuracy. Hu et al. [30] demonstrated that coupling light-responsive materials with enzymatic glucose oxidation enhanced EBFC efficiency, while Rizwan et al. [31] used reliability and sensitivity modeling to identify key factors influencing voltage stability. Parametric sensitivity analysis improves enzymatic biofuel cell design, stability, and performance through mathematical modeling validation. Tamaki et al. [9] used the FDM to solve differential equations in a biofuel cell model. Saravanakumar et al. [32, 33] developed the steady and non-steady state current density using the HPM. To the best of our abilities, no comprehensive analytical formulas for current density and concentrations under non-steady state conditions have been provided for all parameter values.

This study employs the Rajendran-Joy technique [34-37] to derive theoretical results for steady-state current density and concentrations. Our analytical findings enhance the understanding of diffusion and reaction processes in biofuel cell electrodes. These theoretical models assist in experimental planning, parameter optimization, and prediction of electrode behavior. This investigation advances biofuel cell technology by integrating distinct electrode geometries with the Rajendran–Joy method. This integration represents a novel approach that enhances the understanding of electrochemical performance and optimization in biofuel cell systems.

2. The Mathematical Modeling Process

The redox polymer film's enzyme reaction process, which operates on a ping-pong reaction system, can be represented as follows [26]:

$$S + E_{OX} \underset{k_{-1}}{\overset{k_1}{\leftrightarrow}} ES \xrightarrow{k_2} P + E_{Red} \quad \text{(Enzymatic Reaction)} \tag{1}$$

$$2M_{OX} + E_{Red} \xrightarrow{k_{med}} 2M_{Red} + E_{OX} \quad \text{(Mediator-Enzyme Electron Transfer)} \tag{2}$$

The reduced and oxidised forms of the enzyme have been identified as E_{Red} and E_{OX}. Also, M_{OX}/M_{Red} are oxidised and reduced forms of the redox mediator. Herein, S and P represent substrate and product, respectively. The mediator's electron transport at the electrode surface ($x = 0$) may be represented as follows:

$$M_{Red} \leftrightarrow M_{OX} + e^- \quad \text{(Mediator-Electrode Electron Exchange (at } x = 0\text{))} \tag{3}$$

Under steady-state and isothermal conditions, and assuming Fickian diffusion and Michaelis–Menten-type enzymatic reaction kinetics, the system of equations describing the concentration profiles $u(x)$ and $v(x)$ (typically substrate and enzyme-related species) in a general coordinate system (with geometric parameter $N = 0$ for planar, $N = 1$ for cylindrical, and $N = 2$ for spherical geometry) is given by:

$$D_S\left[\frac{1}{x^N}\frac{d}{dx}\left(x^N\frac{dC_S(x)}{dx}\right)\right] - v_{Enz}(C_S, C_{MO}) = 0, \tag{4}$$

$$D_M\left[\frac{1}{x^N}\frac{d}{dx}\left(x^N\frac{dC_{MR}(x)}{dx}\right)\right] + 2v_{Enz}(C_S, C_{MO}) = 0. \tag{5}$$

where C_S and C_{MR} express the concentrations of the substrate (glucose) and the reduced mediator, respectively.

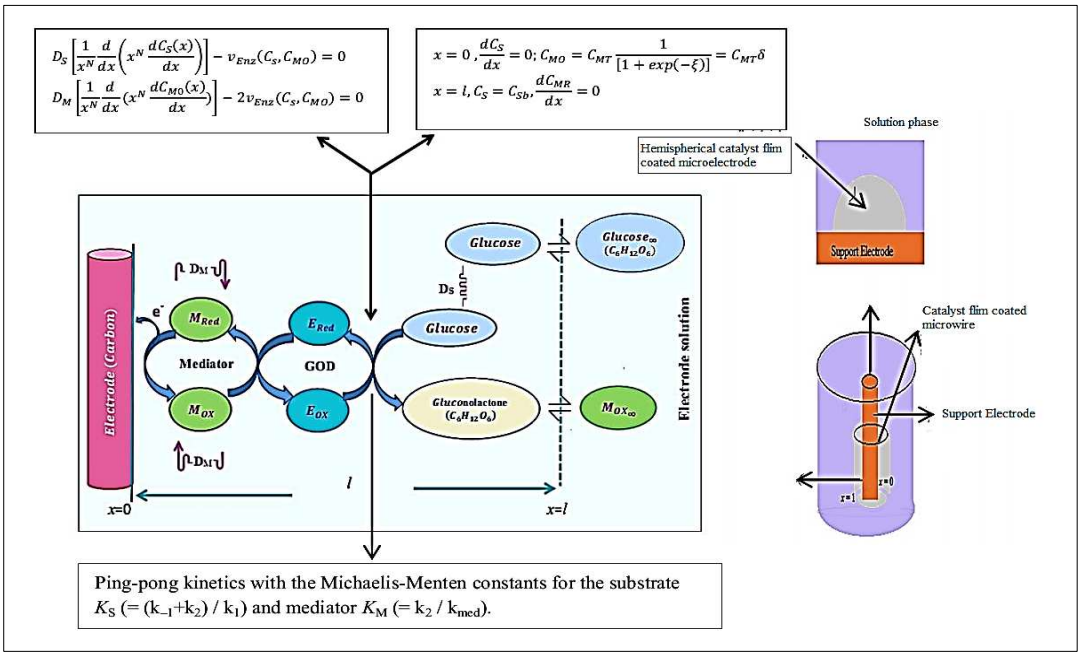

Fig. 1. Engineering design of enzymatic electrode systems for biofuel cells.

The ping-pong process of the rate of reaction of GOD is shown by:

$$\upsilon_{Enz}(C_S, C_{MO}) = \frac{k_{cat} C_{Enz}}{1 + K_S/C_S(x) + K_M/C_{MO}(x)} \tag{6}$$

where C_{Enz} and C_{MO} are the concentrations of the enzyme and the oxidized mediator, respectively, K_S is the Michaelis constant for substrate, and K_M is the Michaelis constant for mediator. All other parameters retain their standard meanings as described in the literature [26]. The boundary conditions are stated below.

At x = 0, (film base or electrode surface):

$$C_S'(x=0) = 0. \quad \text{and} \quad C_{MR}(x=0) = C_{MT}\left[1 + \exp(\xi)\right]^{-1}. \tag{7}$$

At x = 1, (film surface):

$$C_S(x=l) = C_{Sb}. \quad \text{and} \quad C_{MR}'(x=l) = l. \tag{8}$$

Potential $= \xi = nF(E - E^0_{med})/RT$. Also, C_{Sb} represents the bulk concentration of the substrate. At the electrode surface, the current density is:

$$i = nFA_{rp}D_M \left.\frac{dC_{MR}}{dx}\right|_{x=0}, \tag{9}$$

where A_{rp} = (actual surface area) / (predicted surface area). Also, $C_{MR}(x) = C_{MO}(x) = C_{MT} = Q_{MT}/\left(A_{rp}l\right)$ and $C_{Enz} = Q_{ET}/\left(A_{rp}l\right)$. As explained in the texts [26], all the other factors keep their normal meanings. Using the result described above, Eqs. (4) and (5) can be changed into the two subsequent nonlinear differential equations:

$$D_S\left[\frac{1}{x^N}\frac{d}{dx}\left(x^N\frac{dC_s(x)}{dx}\right)\right] - \upsilon_{Enz}(C_S, C_{MO}) = 0, \tag{10}$$

$$D_M\left[\frac{1}{x^N}\frac{d}{dx}\left(x^N\frac{dC_{MO}(x)}{dx}\right)\right] - 2\upsilon_{Enz}(C_S, C_{MO}) = 0. \tag{11}$$

The reaction rate υ_{Enz} is provided by Eq. (6). The boundary conditions are provided by:

$$\text{At } x = 0, \frac{dC_S}{dx} = 0; C_{MO} = C_{MT}\frac{1}{\left[1 + \exp(-\xi)\right]} = C_{MT}\delta, \tag{12}$$

$$\text{At } x = l, C_S = C_{Sb}; \frac{dC_{MO}}{dx} = 0. \tag{13}$$

Here, $1/[1 + \exp(-\xi)] = \delta$. The current density is given below:

$$i = nFA_{rp}D_M \left.\frac{dC_{MO}}{dx}\right|_{x=0}. \tag{14}$$

It is essential to introduce the following dimensionless variables:

$$u(\chi) = \frac{C_S(x)}{C_{Sb}},\ v(\chi) = \frac{C_{MO}(x)}{C_{MT}},\ \chi = \frac{x}{l},\ \phi = \frac{k_{cat}C_{Enz}l^2}{C_{Sb}D_S},\ \alpha = \frac{K_S}{C_{Sb}},\ \beta = \frac{K_M}{C_{MT}}. \tag{15}$$

Equations (10) and (11) become:

$$u''(\chi) + \frac{N}{\chi}u'(\chi) - \frac{\phi u(\chi)v(\chi)}{u(\chi)v(\chi) + \alpha u(\chi) + \beta v(\chi)} = 0. \tag{16}$$

$$v''(\chi) + \frac{N}{\chi}v'(\chi) - \frac{2\phi u(\chi)v(\chi)}{u(\chi)v(\chi) + \alpha u(\chi) + \beta v(\chi)} = 0. \tag{17}$$

The boundary conditions for Eqs. (16) and (17) are defined as follows:

$$u'(\chi = 0) = 0; v(\chi = 0) = \frac{1}{\left[1 + \exp(-\xi)\right]} = \delta. \tag{18}$$

$$u(\chi = 1) = 1;\ v'(\chi = 1) = 0. \tag{19}$$

Nondimensionalization converts Eqs. (4) and (5) into Eqs. (16) and (17) by removing physical units and large parameter variations. This process introduces dimensionless groups like the Thiele modulus, simplifies computation, enhances numerical stability, and generalizes the model for diverse electrode geometries and operating conditions, ensuring broader analytical and practical applicability. The current density is calculated based on the gradient of concentration of the oxidized mediator, as shown in Eq. (20):

$$\psi = \frac{il}{nFA_{rp}D_M} = \left.\frac{dv(\chi)}{dx}\right|_{x=0}. \tag{20}$$

The nonlinear differential equations in (16) and (17) are widely applicable across various scientific and engineering fields involving coupled reaction-diffusion phenomena in radially symmetric domains.

In computational mechanics, this nonlinear diffusion–reaction models are used to simulate coupled transport and reaction phenomena in complex media. They describe heat and mass transfer, chemical reactions, and energy conversion within porous or reactive structures. These models help analyze multiphysics interactions, enabling accurate numerical prediction of thermo-mechanical behavior, material degradation, and performance optimization in engineering systems.

3. Results and Discussion

3.1. A fundamental idea of the Rajendran-Joy Method (RJM)

The Rajendran–Joy Method (RJM) provides an analytical approach for obtaining accurate approximate solutions to nonlinear differential equations. A fundamental idea of RJM [34–37] can be illustrated by considering a nonlinear second-order differential equation with a single independent variable x, expressed as:

$$p_s : f(u_s, u_s', u_s'') = 0;\ s = 1,2,\ldots..,r \tag{21}$$

In this context, p_s denotes a polynomial involving the function $u_S = u_S(x, a, b)$ and its derivatives to x. The parameters a and b are constants, and x belongs to the domain $[L, U]$, which can be either a finite or semi-infinite interval, depending on the problem setting. The function u_S must also satisfy specific boundary conditions:

$$\begin{cases} \text{At } x = L, u_S(x) = u_{SL_0} \text{ or } u_S'(x) = u_{SL_1}. \\ \text{At } x = U, u_S(x) = u_{SU_0} \text{ or } u_S'(x) = u_{SU_1}. \end{cases} \tag{22}$$

Suppose the solution to the nonlinear equations can be expressed as an exponential function:

$$u_S(x) = l_S \exp\left(n_s x^n\right) + m_S \exp\left(-n_s x^n\right) \tag{23}$$

The exponential function is employed because it effectively accommodates boundary conditions that are either finite or semi-infinite. The parameter n is assigned values of 1 or 2, depending on the boundary conditions specified. The values of l_S, m_S and n_S are found by solving the nonlinear equations outlined below:

$$\begin{cases} u_S(L) = l_S \exp(n_S L^n) + m_S \exp(-n_S L^n) = u_{SL_0} \\ \text{or} \\ u_S'(U) = l_S \exp(n_S L^n) - n\, m_S \exp(-n_S L^n) = u_{SU_1} \end{cases} \tag{24}$$

and,

$$\begin{cases} u_S(U) = l_S \exp(n_S U^n) + m_S \exp(-n_S U^n) = u_{SU_0'} \\ \text{or} \\ u_S'(U) = l_S \exp(n_S U^n) - n\, m_S \exp(-n_S U^n) = u_{SU_1'} \end{cases} \tag{25}$$

Inserting Eq. (23) into Eq. (21) yields the following nonlinear algebraic equations:

$$\begin{cases} p_1 : f\left(u_1(x, l_S, m_S, n_S, n, a, b), u_1'(x, l_S, m_S, n_S, n, a, b), u_1''(x, l_S, m_S, n_S, n, a, b)\right) = 0 \\ \ldots \\ p_r : f\left(u_r(x, l_S, m_S, n_S, n, a, b), u_r'(x, l_S, m_S, n_S, n, a, b), u_r''(x, l_S, m_S, n_S, n, a, b)\right) = 0 \end{cases} \tag{26}$$

The preceding equation holds for all x within the interval $[L, U]$. Selecting an arbitrary point $x = \beta$ such that $L \le \beta \le U$, Eq. (26) can be used to derive the following set of linear or nonlinear algebraic equations:

$$\begin{cases} p_1 : f\left(u_1(\beta, l_S, m_S, n_S, n, a, b), u_1'(\beta, l_S, m_S, n_S, n, a, b), u_1''(\beta, l_S, m_S, n_S, n, a, b)\right) = 0 \\ \ldots \\ p_r : f\left(u_r(\beta, l_S, m_S, n_S, n, a, b), u_r'(\beta, l_S, m_S, n_S, n, a, b), u_r''(\beta, l_S, m_S, n_S, n, a, b)\right) = 0 \end{cases} \tag{27}$$

Now the differential equation is converted into a nonlinear algebraic equation. By solving these nonlinear algebraic equations, specifically Eqs. (24), (25), and (27) using Wolfram Alpha, the unknown parameters l_S, m_S and n_S, can be determined for given values of a and b. A flowchart illustrating the basic concept of the RJM method is provided in reference [36].

3.2. Application of the RJM method

Nonlinear equations involving differential variables are the outcome of multidimensional mathematical representations of discrete processes. The Rajendran-Joy method (RJM) may be employed here to solve nonlinear Eqs. (16) and (17). The main benefits of RJM compared to earlier techniques are its simpleness and efficacy in addressing complex nonlinear differential equations. The fundamental principle of this approach is outlined in Section 3.1. Following this method, the solution of the Eqs. (16) and (17) are:

$$u(\chi) = Ae^{m\chi} + Be^{-m\chi}, \tag{28}$$

$$v(\chi) = Ce^{n\chi} + De^{-n\chi}. \tag{29}$$

Applying the boundary conditions from Eqs. (18) and (19) in the above equations, we get:

$$A = B = \frac{1}{\cosh(m)}, \quad C = \frac{\delta e^{-n}}{e^n + e^{-n}} \quad \text{and} \quad D = \frac{\delta e^{-n}}{e^n + e^{-n}} \tag{30}$$

Hence, Eqs. (28) and (29) become as follows:

$$u(\chi)=\frac{\cosh(m\chi)}{\cosh(m)} \tag{31}$$

$$v(\chi)=\frac{\delta\left[\cosh\left((1-\chi)n\right)\right]}{\cosh(n)} \tag{32}$$

Substituting Eqs. (31) and (32) in Eq. (16) and simplifying the result at $x = 1$, we get:

$$m^2=\left(\frac{\delta\phi}{(1+N)(\delta+\alpha\delta+\beta)}\right) \tag{33}$$

In addition, if we use Eqs. (31) and (32) in Eq. (17) and simplify the outcome for $x = 0.5$, we obtain:

$$n^2=\left(\frac{2\phi}{(1+N)(\delta+\alpha\delta+\beta)}\right) \tag{34}$$

Dimensionless current is:

$$\psi=\delta n\tanh(n)\approx\delta n^2=\delta\left[\frac{2\phi}{(1+N)(\delta+\alpha\delta+\beta)}\right] \tag{35}$$

From Eq. (35), it is observed that the dimensionless current ψ is most sensitive to the kinetic parameter ϕ and the mass transfer term N, which directly govern reaction and transport rates. Parameters δ, α, and β significantly influence performance depending on their relative magnitudes, with $\beta/\delta(1+\alpha)$ determining diffusion–reaction dominance in the biofuel cell.

When $\xi=-\infty$,

$$\delta=\frac{1}{\left[1+\exp(-\xi)\right]}=0 \text{ and } n=\sqrt{\frac{2\phi}{\beta(1+N)}}, \text{ the current } \psi(\xi=-\infty)=0.$$

Similarly, when $\xi=\infty$,

$$\delta=\frac{1}{\left[1+\exp(-\xi)\right]}=1. \text{ Current is } \psi(\xi=\infty)=\frac{2\phi}{\left[(1+N)(1+\alpha+\beta)\right]}.$$

The electric power of fuel cell is $P = i^2R$. Here R is the external resistance and:

$$\mathrm{i}=nFA_{rp}D_M\delta\left[\frac{2\phi}{(1+N)(\delta+\alpha\delta+\beta)}\right]. \tag{36}$$

The power becomes, $P=\left[nFA_{rp}D_M\right]^2\left[\frac{2\delta\phi}{(1+N)(\delta+\alpha\delta+\beta)}\right]^2 R$. Now the dimensionless power p becomes:

$$p=\frac{P}{R\left[nFA_{rp}D_M\right]^2}=\left[\frac{2\delta\phi}{(1+N)(\delta+\alpha\delta+\beta)}\right]^2. \tag{37}$$

3.3. Validation of analytical results with numerical results

The nonlinear differential Eq. (16) and (17) are solved using the function pdexred in Scilab, a numerical software (Free and open-source software for numerical computation. Available: https://www.scilab.org). The analytical solutions (Eqs. (28) and (29)) are compared with the numerical results in Figs. 1 and 2 and Tables 1-8 for various experimental values of parameters. The new analytical and simulated results are very close. In addition, the average error between the numerical and analytical results is only 0.5%, highlighting the high accuracy and robustness of the proposed model. This small deviation confirms that the analytical formulation can reliably predict the performance of biofuel cells under various operating conditions.

3.3.1. *Effect of the parameter on the substrate concentration at the electrode surface*

The general analytical equations for the concentrations of substrate and oxidized mediator are represented by Eqs. (31) and (32). One of the most important parameters in mass transfer is the substrate concentration at the electrode surface. The electrode surface concentration fundamentally determines the coupling efficiency between enzymatic reactions and electron transfer in biofuel cells. Engineering design must integrate reaction–diffusion modelling, material optimization, and system-level mass transport control to achieve maximal performance. Neglecting surface concentration effects leads to inaccurate modelling, poor power prediction, and suboptimal fuel utilization

The type dependency of the error function determines the substrate concentration for simple diffusion-controlled processes in potential step experiments. However, because it relies on the scan rate, the equations for the surface concentration in cyclic voltametric studies are more complex. The surface concentrations of ultramicroelectrodes depend on the process being studied and the electrode shape. Therefore, the accurate expression for surface concentrations concerning electrochemical analysis is essential to understanding the reaction process. In our problem (from Eq. (28)) the concentration of the substrate at $\chi = 0$ is:

$$u(\chi=0)=\operatorname{sech}\left(\sqrt{\frac{\delta\phi}{(1+N)(\delta+\alpha\delta+\beta)}}\right). \tag{38}$$

Table 1. Comparison of numerical and analytical (RJM) results for $u(\chi)$ at various values of ϕ when $\delta = 0.8$, $\beta = 3$, $\alpha = 15$, $N = 0$.

χ	Numerical				RJM Eq. (31)				Error %			
	$\phi = 0.01$	$\phi = 1$	$\phi = 3$	$\phi = 5$	$\phi = 0.01$ $m = 0.0225$ $n = 0.0356$	$\phi = 1$ $m = 0.0236$ $n = 0.3653$	$\phi = 3$ $m = 0.3814$ $n = 0.6695$	$\phi = 5$ $m = 0.4828$ $n = 0.9206$	$\phi = 0.01$	$\phi = 1$	$\phi = 3$	$\phi = 5$
0.0	0.9997	0.9753	0.9288	0.8863	0.9997	0.9755	0.9314	0.8938	0.0000	0.0205	0.2799	0.8462
0.2	0.9997	0.9763	0.9318	0.8910	0.9997	0.9765	0.9342	0.8981	0.0000	0.0205	0.2576	0.7969
0.4	0.9997	0.9793	0.9405	0.9049	0.9997	0.9795	0.9425	0.9109	0.0000	0.0204	0.2127	0.6631
0.6	0.9997	0.9843	0.9550	0.9281	0.9997	0.9845	0.9564	0.9323	0.0000	0.0203	0.1466	0.4525
0.8	0.9997	0.9914	0.9753	0.9605	0.9997	0.9915	0.9760	0.9627	0.0000	0.0101	0.0718	0.2290
1.0	0.9997	1.0000	1.0000	1.0000	0.9997	1.0000	1.0000	1.0000	0.0000	0.0000	0.0000	0.0000
							Average Error %		0.0000	0.0153	0.1614	0.4980

Table 2. Comparison of numerical and analytical (RJM) results for $u(\chi)$ at various values of α when $\delta = 0.8$, $\phi = 5$, $\beta = 3$, $N = 0$.

χ	Numerical				RJM Eq. (31)				Error %			
	$\alpha = 15$	$\alpha = 30$	$\alpha = 100$	$\alpha = 10000$	$\alpha = 15$ $m = 0.4828$ $n = 0.9206$	$\alpha = 30$ $m = 0.3748$ $n = 0.6553$	$\alpha = 100$ $m = 0.2182$ $n = 0.3559$	$\alpha = 10000$ $m = 0.0224$ $n = 0.0354$	$\alpha = 15$	$\alpha = 30$	$\alpha = 100$	$\alpha = 10000$
0.0	0.8863	0.9323	0.9766	0.9998	0.8938	0.9336	0.9767	0.9998	0.8462	0.1394	0.0102	0.0000
0.2	0.8910	0.9350	0.9776	0.9998	0.8981	0.9363	0.9776	0.9998	0.7969	0.1390	0.0000	0.0000
0.4	0.9049	0.9433	0.9804	0.9998	0.9109	0.9444	0.9805	0.9998	0.6631	0.1166	0.0102	0.0000
0.6	0.9281	0.9571	0.9852	0.9998	0.9323	0.9578	0.9852	0.9998	0.4525	0.0731	0.0000	0.0000
0.8	0.9605	0.9764	0.9919	0.9998	0.9627	0.9768	0.9919	0.9998	0.2290	0.0410	0.0000	0.0000
1.0	1.0000	1.0000	1.0000	0.9998	1.0000	1.0000	1.0000	0.9998	0.0000	0.0000	0.0000	0.0000
							Average Error %		0.4980	0.0849	0.0034	0.0000

Table 3. Comparison of numerical and analytical (RJM) results for $u(\chi)$ at various values of β when $\delta = 0.8$, $\phi = 5$, $\alpha = 15$, $N = 0$.

χ	Numerical				RJM Eq. (31)				Error %			
	$\beta = 3$	$\beta = 15$	$\beta = 50$	$\beta = 5000$	$\beta = 3$ $m = 0.4828$ $n = 0.9206$	$\beta = 15$ $m = 0.3603$ $n = 0.6243$	$\beta = 50$ $m = 0.2445$ $n = 0.4022$	$\beta = 5000$ $m = 0.0282$ $n = 0.0447$	$\beta = 3$	$\beta = 15$	$\beta = 50$	$\beta = 5000$
0.0	0.8863	0.9331	0.9693	0.9996	0.8938	0.9384	0.9708	0.9996	0.8462	0.5680	0.1548	0.0000
0.2	0.8910	0.9359	0.9706	0.9996	0.8981	0.9409	0.9720	0.9996	0.7969	0.5342	0.1442	0.0000
0.4	0.9049	0.9442	0.9744	0.9996	0.9109	0.9484	0.9756	0.9996	0.6631	0.4448	0.1232	0.0000
0.6	0.9281	0.9580	0.9807	0.9996	0.9323	0.9609	0.9815	0.9996	0.4525	0.3027	0.0816	0.0000
0.8	0.9605	0.9770	0.9894	0.9996	0.9627	0.9785	0.9898	0.9996	0.2290	0.1535	0.0404	0.0000
1.0	1.0000	1.0000	1.0000	0.9996	1.0000	1.0000	1.0000	0.9996	0.0000	0.0000	0.0000	0.0000
							Average Error %		0.4980	0.3339	0.0907	0.0000

Table 4. Comparison of numerical and analytical (RJM) results for $u(\chi)$ at various values of δ when $\beta = 3$, $\phi = 5$, $\alpha = 15$, $N = 0$.

χ	Numerical				RJM Eq. (31)				Error %			
	$\delta = 0.0001$	$\delta = 0.1$	$\delta = 0.5$	$\delta = 1$	$\delta = 0.0001$ $m = 0.0072$ $n = 1.8256$	$\delta = 0.1$ $m = 0.2252$ $n = 1.6710$	$\delta = 0.5$ $m = 0.4353$ $n = 1.1454$	$\delta = 1$ $m = 0.4991$ $n = 0.8224$	$\delta = 0.0001$	$\delta = 0.1$	$\delta = 0.5$	$\delta = 1$
0	1	0.9596	0.8998	0.8814	1	0.9752	0.9122	0.8872	0	1.6257	1.3781	0.658
0.2	1	0.9617	0.9041	0.8862	1	0.9762	0.9157	0.8917	0	1.5077	1.283	0.6206
0.4	1	0.9674	0.9166	0.9007	1	0.9792	0.9263	0.9053	0	1.2198	1.0583	0.5107
0.6	1	0.9761	0.9372	0.9248	1	0.9843	0.9441	0.9281	0	0.8401	0.7362	0.3568
0.8	1	0.9873	0.9657	0.9586	1	0.9914	0.9692	0.9603	0	0.4153	0.3624	0.1773
1	1	1	1	1	1	1	1	1	0	0	0	0
							Average Error %		0	0.9348	0.803	0.3873

Table 5. Comparison of numerical and analytical (RJM) results for $v(\chi)$ for various values of ϕ when $\delta = 1$, $\beta = 3$, $\alpha = 0.01$, $N = 0$.

χ	Numerical				RJM Eq. (32)				Error %			
	$\phi = 0.01$	$\phi = 1.5$	$\phi = 3$	$\phi = 5$	$\phi = 0.01$ $m = 0.0499$ $n = 0.0706$	$\phi = 1.5$ $m = 0.5316$ $n = 0.8999$	$\phi = 3$ $m = 0.6565$ $n = 1.3076$	$\phi = 5$ $m = 0.7171$ $n = 1.7283$	$\phi = 0.01$	$\phi = 1.5$	$\phi = 3$	$\phi = 5$
0	1	1	1	1	1	1	1	1	0	0	0	0
0.2	0.9991	0.8879	0.8104	0.7378	0.9991	0.8856	0.8043	0.7271	0	0.259	0.7527	1.4503
0.4	0.9984	0.8038	0.6729	0.5562	0.9984	0.8006	0.665	0.5437	0	0.3981	1.174	2.2474
0.6	0.9979	0.7455	0.5802	0.4388	0.9979	0.7422	0.5724	0.4272	0	0.4427	1.3444	2.6436
0.8	0.9976	0.7116	0.5274	0.3737	0.9976	0.7083	0.52	0.3634	0	0.4637	1.4031	2.7562
1	0.9975	0.7011	0.5113	0.3541	0.9975	0.6979	0.5041	0.3443	0	0.4564	1.4082	2.7676
							Average Error %		0	0.3367	1.0137	1.9775

Table 6. Comparison of numerical and analytical (RJM) results for $v(\chi)$ for various values of α when $\delta = 1$, $\phi = 5$, and $\beta = 3$, N = 0.

χ	Numerical				RJM Eq. (32)				Error %			
	$\alpha = 0.01$	$\alpha = 10$	$\alpha = 40$	$\alpha = 10000$	$\alpha = 0.01$ $m = 0.7171$ $n = 1.7283$	$\alpha = 10$ $m = 0.5662$ $n = 0.9913$	$\alpha = 40$ $m = 0.3356$ $n = 0.5045$	$\alpha = 10000$ $m = 0.0224$ $n = 0.0316$	$\alpha = 0.01$	$\alpha = 10$	$\alpha = 40$	$\alpha = 10000$
0	1	1	1	1	1	1	1	0.9997	0	0	0	0.03
0.2	0.7378	0.8867	0.9602	1	0.7271	0.8673	0.9577	0.9997	1.4503	2.1879	0.2604	0.03
0.4	0.5562	0.7987	0.9293	1	0.5437	0.7695	0.9253	0.9997	2.2474	3.6559	0.4304	0.03
0.6	0.4388	0.7359	0.9072	1	0.4272	0.7027	0.9025	0.9997	2.6436	4.5115	0.5181	0.03
0.8	0.3737	0.6983	0.894	1	0.3634	0.6642	0.8891	0.9997	2.7562	4.8833	0.5481	0.03
1	0.3541	0.6865	0.8899	1	0.3443	0.6523	0.885	0.9997	2.7676	4.9818	0.5506	0.03
							Average Error %		1.9775	3.3701	0.3846	0.03

Table 7. Comparison of numerical and analytical (RJM) results for $v(\chi)$ for various values of β when $\delta = 1$, $\phi = 5$, $\alpha = 0.01$, N = 0.

χ	Numerical				RJM Eq. (32)				Error %			
	$\beta = 3$	$\beta = 10$	$\beta = 40$	$\beta = 5000$	$\beta = 3$ $m = 0.7171$ $n = 1.7283$	$\beta = 10$ $m = 0.5577$ $n = 0.9681$	$\beta = 40$ $m = 0.3297$ $n = 0.4945$	$\beta = 5000$ $m = 0.0316$ $n = 0.0447$	$\beta = 3$	$\beta = 10$	$\beta = 40$	$\beta = 5000$
0	1	1	1	1	1	1	1	0.9995	0	0	0	0.05
0.2	0.7378	0.873	0.9592	1	0.7271	0.872	0.9592	0.9995	1.4503	0.1145	0	0.05
0.4	0.5562	0.7788	0.928	1	0.5437	0.7774	0.928	0.9995	2.2474	0.1798	0	0.05
0.6	0.4388	0.7141	0.906	1	0.4272	0.7127	0.906	0.9995	2.6436	0.1961	0	0.05
0.8	0.3737	0.6767	0.8931	1	0.3634	0.6754	0.8931	0.9995	2.7562	0.1921	0	0.05
1	0.3541	0.6652	0.8891	1	0.3443	0.6639	0.8891	0.9995	2.7676	0.1954	0	0.05
							Average Error %		1.9775	0.1463	0	0.05

Table 8. Comparison of numerical and analytical (RJM) results for $v(\chi)$ for various values of δ when $\phi = 5$, $\beta = 3$, $\alpha = 0.01$, N = 0.

χ	Numerical			RJM Eq. (32)			Error %		
	$\delta = 0.01$	$\delta = 0.5$	$\delta = 1$	$\delta = 0.01$ $m = 0.0723$ $n = 1.8248$	$\delta = 0.5$ $m = 0.5095$ $n = 1.7772$	$\delta = 1$ $m = 0.7171$ $n = 1.7273$	$\delta = 0.01$	$\delta = 0.5$	$\delta = 1$
0	0.01	0.5	1	0.01	0.5	1	0	0	0
0.2	0.0071	0.3624	0.7378	0.0071	0.3594	0.7271	0	0.8278	1.4503
0.4	0.0052	0.269	0.5562	0.0052	0.2656	0.5437	0	1.2639	2.2474
0.6	0.0039	0.2094	0.4388	0.0039	0.2064	0.4272	0	1.4327	2.6436
0.8	0.0033	0.1767	0.3737	0.0033	0.1741	0.3634	0	1.4714	2.7562
1	0.0031	0.1669	0.3541	0.0031	0.1644	0.3443	0	1.4979	2.7676
						Average Error %	0	1.0823	1.9775

From Eq. (38), it is observed that the maximum value of the concentration of substrate at the electrode surface is one. This maximum value is also reached when α, β, and N are large while ϕ and δ are incredibly small.

The mathematical ceiling implied by Eq. (38) unity surface concentration under optimised kinetics and transport defines a tangible engineering target. By manipulating electrode microgeometry, flow architecture and operating conditions to elevate α, β, N while suppressing ϕ, δ practitioners can approach this limit, translating directly into higher current densities, sharper selectivity and lower specific energy consumption. Modern tools such as 3D printing, CFD optimisation and integrated micro-sensing now make these ideals practically attainable, heralding more efficient, scalable and robust electrochemical technologies.

3.3.2. Impact of the parameters on the concentrations

The concentration of the mediator and substrate is determined by the parameter *m,* which in turn is controlled by the variables ϕ, α, β, and δ. The parameter ϕ represents the Thiele modulus. The kinetics dominate, and the substrate uptake is kinetically regulated when the Thiele modulus is relatively small. Internal diffusion is rate-limiting for high Thiele modulus values, which causes the concentration in the enzyme layer to decrease rapidly to nearly zero. The kinetic parameters α and β are directly proportional to the Michaelis constant and bulk concentration of substrate and mediator. Also, the parameter δ is directly proportional to the potential. This finding indicates that optimizing the Thiele modulus, for example by adjusting the enzyme film thickness, can enhance biofuel cell efficiency through a balanced interaction between diffusion and reaction rates.

The fluctuation of the substrate concentration for various system parameters is determined by Eq. (31), is shown in Figs. 2(a)-2(d). It is evident from Fig. 2(a) that when the Thiele modulus increases, the substrate concentration value decreases. As the Thiele modulus increases, the substrate concentration decreases, indicating that diffusion becomes the rate-limiting step at higher moduli, thereby reducing the overall efficiency of the biofuel cell. Substrate surface concentration increases with kinetic parameters α (enzymatic rate) and β (electron transfer rate), or when bulk substrate decreases, creating favorable diffusion gradients (Figs. 1(b), 1(c)). The resulting potential drop with higher surface concentration (Fig. 2(d)) reflects Nernst thermodynamics, where increased substrate availability reduces oxidation potential but enhances current generation—a fundamental voltage-current trade-off in bioelectrocatalytic systems. Also, the concentration is uniform when $\phi < 0.01$ and $\delta < 0.01$. The variation of the oxidized mediator concentration $v(\chi)$ with system parameters is illustrated in Figs. 3(a)-(d). Figure 3(a) shows that increasing the Thiele modulus reduces $v(\chi)$, reflecting enhanced substrate diffusion limitations and reaction confinement within the electrode. In Fig. 3(b), higher substrate Michaelis–Menten constants increase $v(\chi)$, indicating slower enzymatic consumption of substrate and accumulation of the oxidized mediator. Figure 3(c) reveals that decreasing the mediator Michaelis–Menten constant lowers $v(\chi)$, as faster mediator turnover accelerates electron transfer. Across Figs. 3(a)-(c), reductions in both α and β decrease $v(\chi)$, reflecting the combined effects of limited diffusion and reaction kinetics. Figure 3(d) demonstrates that higher applied potentials elevate $v(\chi)$ by driving the oxidation of the mediator more strongly, consistent with electrochemical control of the biofuel cell.

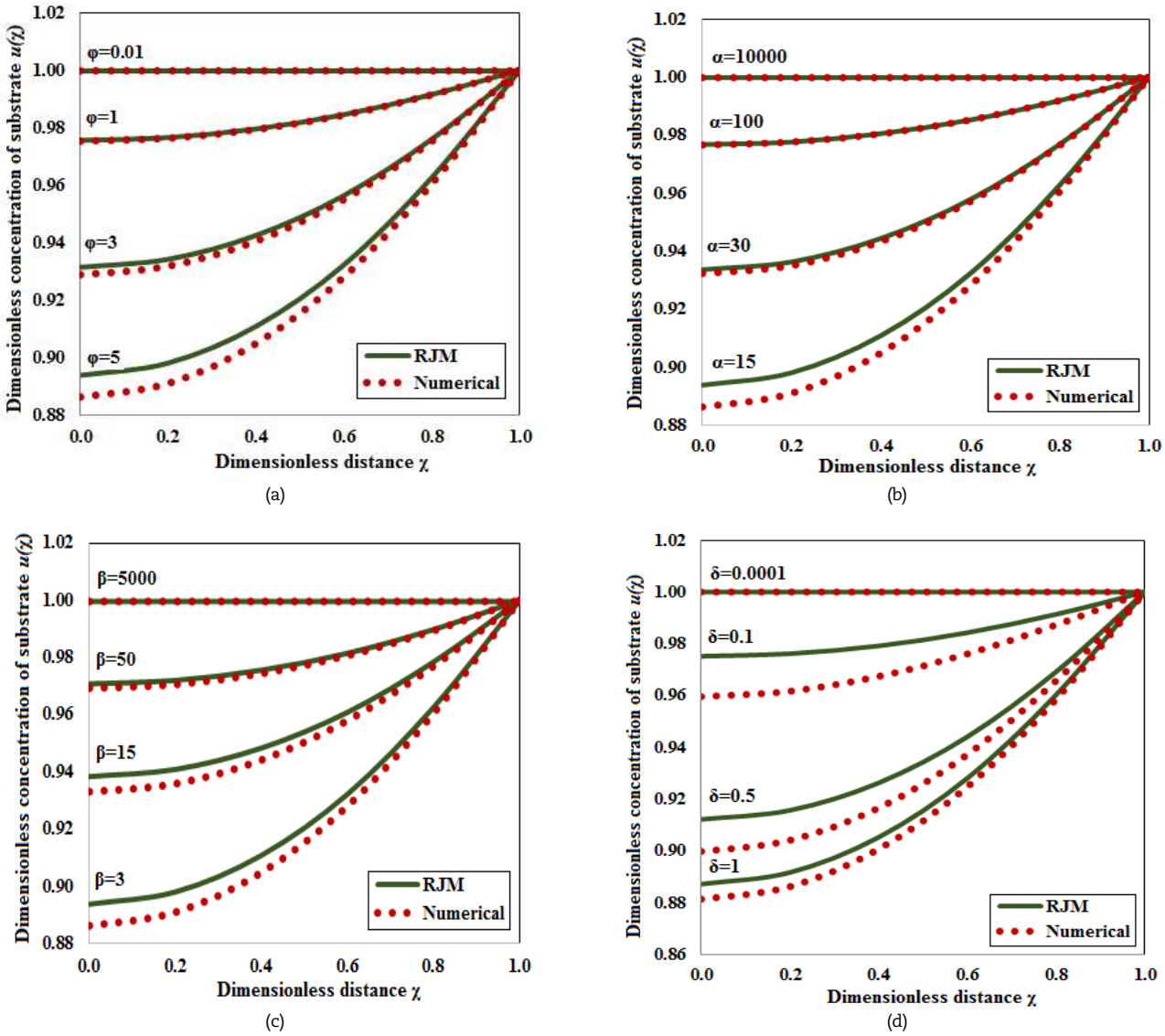

Fig. 2. Effect of (a) Thiele modulus ϕ for δ = 0.8, β = 3, α = 15, (b) Michaelis constant (substrate) α for δ = 0.8, ϕ = 5, β = 3, (c) Michaelis constant (mediator) β for δ = 0.8, ϕ = 5, α = 15, (d) dimensional potential δ for ϕ = 5, β = 3, α = 15 on dimensionless substrate concentration of planar particle.

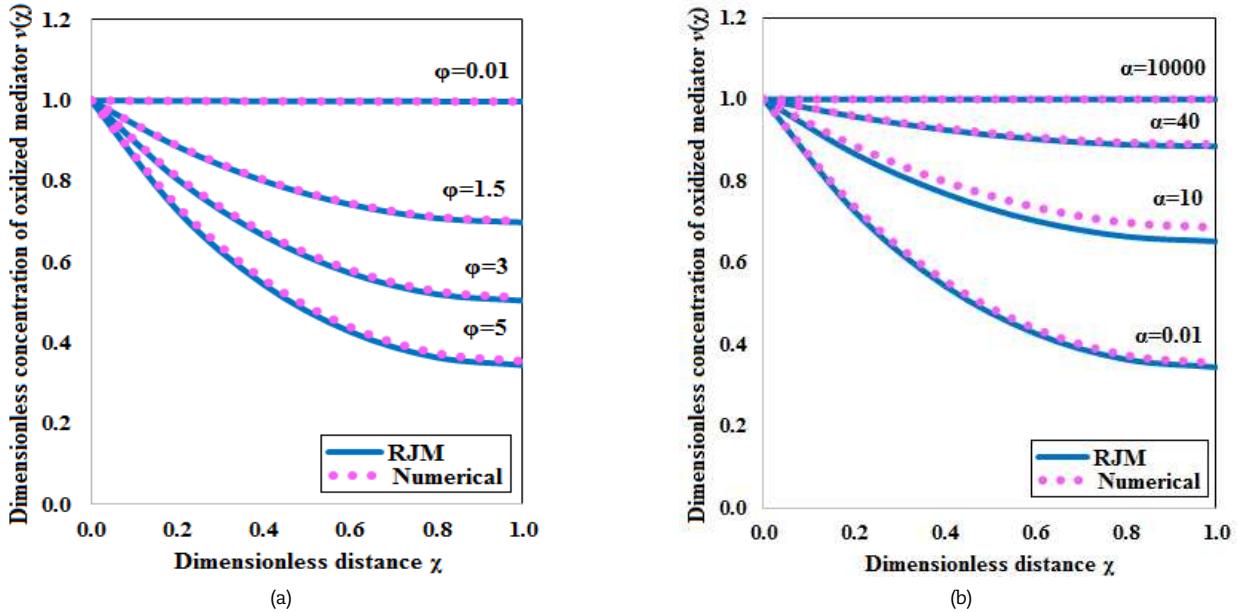

Fig. 3. Effect of (a) Thiele modulus ϕ for δ = 1, β = 3, α = 0.01, (b) Michaelis constant (substrate) α for δ = 1, ϕ = 5, β = 3, (c) Michaelis constant (mediator) β for δ = 1, ϕ = 5, α = 0.01 (d) potential δ for ϕ = 5, β = 3, α = 0.01 on dimensionless mediator concentration of planar particle.

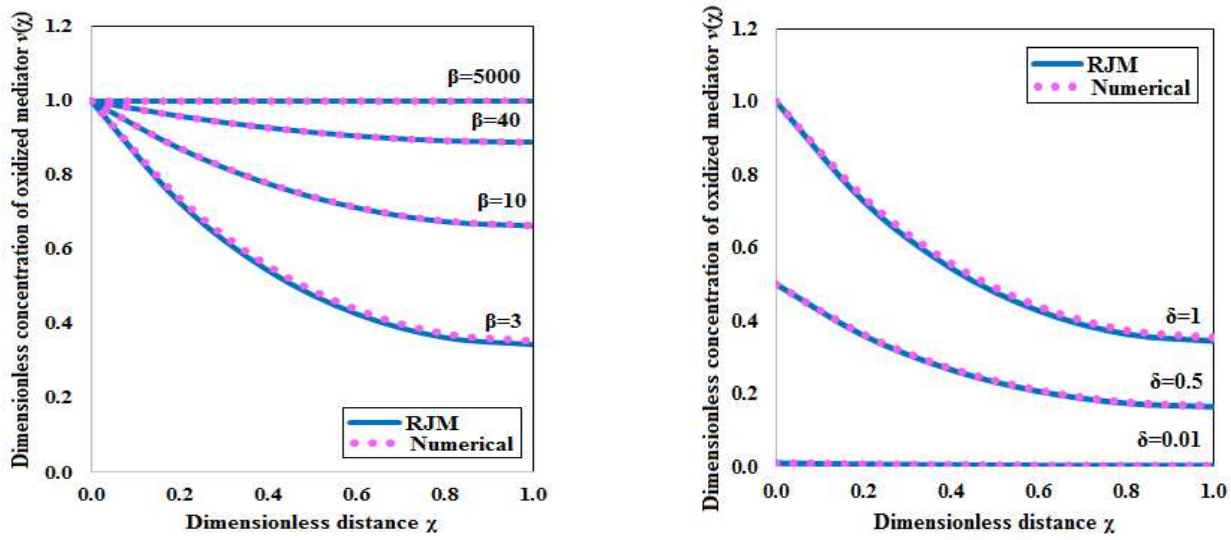

(c) (d)

Fig. 3. Continued.

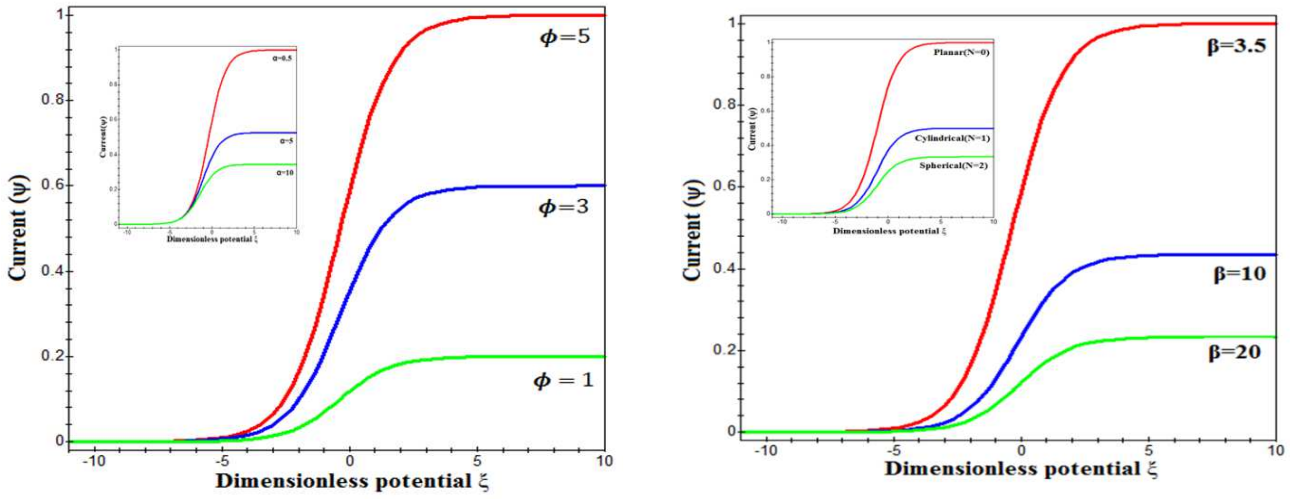

(a) (b)

Fig. 4. Current density ψ versus potential for various values of parameters when (a) $\beta = 3.5$, $\alpha = 0.5$, $N = 1$ (a. inner diagram); $\beta = 3.5$, $\phi = 5$, $N = 1$, (b) $\alpha = 0.5$, $\phi = 5$, $N = 1$ (b. inner diagram); $\beta = 3.5$, $\alpha = 5.5$, $\phi = 5$.

3.3.3. *Effect of the parameters on the current*

Figure 4(a) represents the effect of the Thiele modulus and kinetic parameters α on current. From Fig. 4(a), it is evident that the current increases when the turnover rate, Thiele modulus or increases. Figures 4(a) and 4(b) show that the current density decreases upon an increase in the kinetic parameters α, β values. Figure 4(b) displays the effects of the shape factor and the kinetic parameter β of the current density. An increase in the shape factor leads to a reduction in current density. Figure 4(a-b) shows the fluctuation of the steady-state current density for various potential levels. The current density is minimum at a large negative potential. All combined data are displayed in these figures, demonstrating how the current density rises as the potential increases for all other parameter values. Furthermore, the highest value of the current density is reached when the dimensionless potential $\xi = 5$. The results indicate that electrode geometry has a substantial effect on biofuel cell efficiency, with cylindrical and spherical configurations outperforming planar ones at higher Thiele modulus values. This suggests that the selection of electrode geometry should be tailored to the specific operating conditions and diffusion characteristics of the biofuel cell.

3.3.4. *Effect of the parameters on the power*

The plot of power versus potential for different parameter values using Eq. (37) are shown in Figs 5(a) and 5(b). As the bulk concentration of glucose increases, the power attained its maximum. There is a correlation between decreasing film thickness and increasing power density.

Figure 5(a) represents the effect of the Thiele modulus on power. From Fig. 5(a), it is observed that the current increases when the turnover rate, Thiele modulus, increases. Figures 5(a) and 5(b) illustrate that power diminishes as the kinetic parameters α and β increase. Figure 5(b) displays the effects of the shape factor on the power. As the shape factor increases, the power output of enzymatic biofuel cells tends to decrease. This is largely due to greater mass transfer limitations and less efficient utilization of the electrode surface. A higher shape factor impedes the diffusion of fuel and oxygen to the enzyme sites, thereby limiting the reaction kinetics. Consequently, the reduced accessibility and active surface area lead to lower rates of electrochemical reactions and diminished overall power generation efficiency.

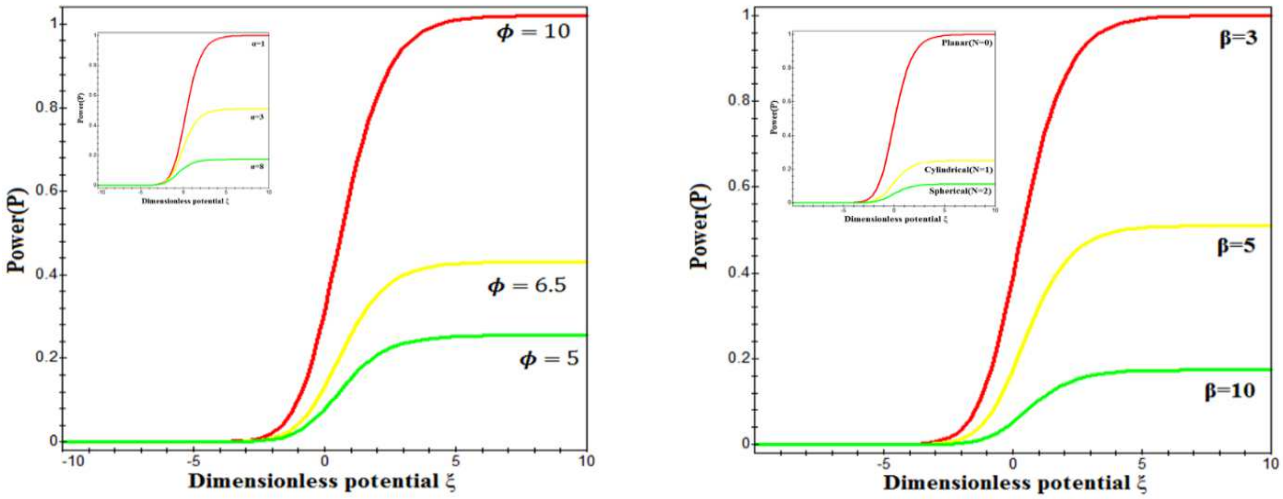

(a) (b)

Fig. 5. Dimensionless Power versus potential for various values of parameters when (a) $\beta = 8$, $\alpha = 0.9$, $N = 1$, (b) $\alpha = 1$, $\phi = 5$, $N = 1$.

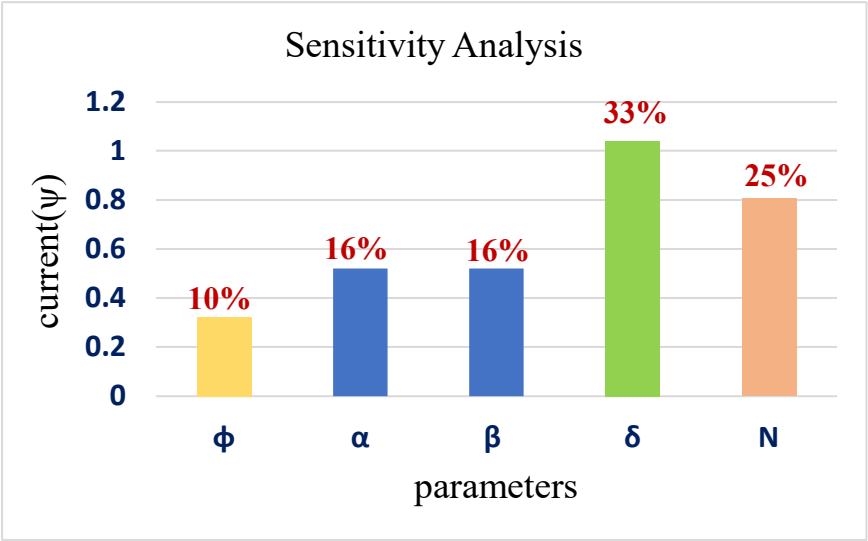

Fig. 6. Sensitivity analysis of parameters: Percentage change in current density ψ for $\alpha = 0.1$, $\beta = 2$, $\delta = 1$, $\phi = 5$, $N = 1$.

3.4. Differential sensitivity analysis of parameters

The differential equation of the model is the key to differential sensitivity analysis. The partial derivative of the dependent variable (current density) has been determined about the independent variables (ϕ, α, β, δ, and N). One may obtain the numerical value of the rate of change of the current density, ψ, at specific experimental values ($\alpha = 0.1$, $\beta = 2$, $\delta = 1$, $\phi = 5$, and $N = 1$) of the parameters. The percentage of change in current density concerning the parameters can be determined from this value. Figure 5 provides a sensitivity analysis of the parameters.

It may be seen from Fig. 6 that the parameter δ (potential) and N (Shape factor) are highly significant. Since δ (Potential) is critical for driving efficient electron transfer and maximizing bioelectrocatalytic activity, and N (Shape Factor) controls geometric optimization of mass transfer and reaction surface area, directly affecting power output and efficiency. The current density in a biofuel cell shows little variation with Thiele modulus, Michaelis-Menten constant, and kinetic parameters because the system often operates under diffusion-limited conditions. In such cases, mass transport dominates the reaction rate, minimizing the influence of kinetic factors.

The global Sobol sensitivity analysis or the Morris method will also be applied to analyse the parameters. Sobol's method is a variance-based global sensitivity analysis technique. It decomposes the total variance of a model output into fractions attributed to individual inputs and their interactions. The Morris method is a screening method for identifying which input parameters have significant, negligible, or non-linear effects.

3.5. Various limiting cases

The rate of a reaction and its dependence on reactant concentration are characterized by Michaelis-Menten, zero-order, and first-order kinetics.

Limiting case 1 (Michaelis-Menten kinetics): When $K_M << C_{MT}$ or β is very small, the rate of the reaction becomes Michaelis-Menten kinetics. Now the Eqs. (16) and (17) reduce to:

$$u''(\chi)+\frac{N}{\chi}u'(\chi)-\frac{\phi u(\chi)}{u(\chi)+\alpha}=0. \text{ and } v''(\chi)+\frac{N}{\chi}v'(\chi)-\frac{2\phi u(\chi)}{u(\chi)+\alpha}=0. \tag{39}$$

The concentrations are obtained by using the boundary conditions (18) and (19) as:

$$u(\chi)=\frac{\cosh\left(\sqrt{\left(\frac{\phi}{(1+N)(1+\alpha)}\right)}\chi\right)}{\cosh\left(\sqrt{\left(\frac{\phi}{(1+N)(1+\alpha)}\right)}\right)} \quad \text{and} \quad v(\chi)=\frac{\delta\left[\cosh\left((1-\chi)\sqrt{\left(\frac{2\phi}{\delta(1+N)(1+\alpha\delta)}\right)}\right)\right]}{\cosh\left(\sqrt{\left(\frac{2\phi}{\delta(1+N)(1+\alpha\delta)}\right)}\right)}. \tag{40}$$

The current is:

$$\psi=\left[\frac{2\phi}{(1+N)(1+\alpha)}\right]. \tag{41}$$

Limiting case 2 (First-Order Kinetics): When $K_M << C_{MT}$, and $C_{sb} << K_S$, the reaction is first-order kinetics. In this case, $\beta = 0$ and α is large, and the Eqs. (16) and (17) become:

$$u''(\chi)+\frac{N}{\chi}u'(\chi)-\frac{\phi}{\alpha}u(\chi)=0. \quad \text{and} \quad v''(\chi)+\frac{N}{\chi}v'(\chi)-\frac{2\phi}{\alpha}u(\chi)=0. \tag{42}$$

The concentrations are determined by applying boundary conditions (18) and (19) as:

$$u(\chi)=\begin{cases}\dfrac{\cosh\left(\sqrt{\left(\frac{\phi}{\alpha}\right)}\chi\right)}{\cosh\left(\sqrt{\left(\frac{\phi}{\alpha}\right)}\right)}, & N=0\\ \dfrac{J_0\left(i\frac{\sqrt{\phi}}{\sqrt{\alpha}}\chi\right)}{J_0\left(i\frac{\sqrt{\phi}}{\sqrt{\alpha}}\right)}, & N=1\\ \dfrac{\sinh\left(\sqrt{\left(\frac{\phi}{\alpha}\right)}\chi\right)}{\chi\sinh\left(\sqrt{\left(\frac{\phi}{\alpha}\right)}\right)}, & N=2\end{cases} \quad \text{and} \quad v(\chi)=\frac{\delta\left[\cosh\left((1-\chi)\sqrt{\left(\frac{2\phi}{\delta(1+N)\alpha\delta}\right)}\right)\right]}{\cosh\left(\sqrt{\left(\frac{2\phi}{\delta(1+N)}\right)}\right)} \tag{43}$$

The current is:

$$\psi=\left[\frac{2\phi}{(1+N)\alpha}\right]. \tag{44}$$

Limiting case 3 (Zero-Order Kinetics): In zero-order kinetics, the reaction rate does not depend on reactant concentration, and a fixed amount of the reactant is removed per unit time. In this case, $C_{sb} >> K_S$ and $C_{MT} >> K_M$ or $\alpha = 0$, $\beta = 0$. Now the Eqs. (16) and (17) become:

$$u''(\chi)+\frac{N}{\chi}u'(\chi)-\phi=0. \quad \text{and} \quad v''(\chi)+\frac{N}{\chi}v'(\chi)-2\phi=0. \tag{45}$$

Applying the boundary conditions (18) and (19) gives us the concentrations:

$$u(\chi)=\frac{2N+\phi x^2-\phi+2}{2} \quad \text{and} \quad v(\chi)=\frac{\delta\left[\cosh\left((1-\chi)\sqrt{\left(\frac{2\phi}{\delta(1+N)}\right)}\right)\right]}{\cosh\left(\sqrt{\left(\frac{2\phi}{\delta(1+N)}\right)}\right)}. \tag{46}$$

From this, we can get the appropriate current as:

$$\psi=\left[\frac{2\phi}{(1+N)}\right]. \tag{47}$$

The present findings provide a robust analytical framework for predicting enzymatic biofuel cell behavior, guiding experimental validation and optimization of electrode design. Future research may extend this model to transient or multi-enzyme systems, integrate heterogeneous electron transfer kinetics, and support advanced theoretical developments for next-generation bioelectrochemical energy devices.

4. Conclusion

In this study, a comprehensive mathematical model was developed to describe nonlinear reaction–diffusion processes occurring at electrodes of various geometries in enzymatic biofuel cells. By integrating Michaelis–Menten-type enzyme kinetics and applying the Rajendran–Joy analytical method, explicit solutions were obtained for substrate and mediator concentration profiles. The analysis revealed that the dimensionless current is strongly influenced by the Thiele modulus, catalytic rate constants, enzyme loading, applied potential, and electrode geometry- key factors determining biofuel cell efficiency and design optimization. Beyond biofuel cell performance analysis, the proposed modelling framework has wide-ranging applicability. It can be directly employed in designing enzyme-based biosensors for medical diagnostics, optimizing controlled drug release systems, enhancing enzyme-reactor configurations in bioprocess engineering, and simulating nutrient transport in tissue scaffolds. Moreover, it can

aid in predicting pollutant degradation in environmental systems and studying thermochemical reactions in energy materials. A more detailed exploration of these practical applications in future studies would further strengthen the model's impact and promote its integration into experimental and industrial design strategies.

Author Contributions

R. Rajalakshmi contributed to the Methodology, Software, Writing – original draft. A. Marimuthu was responsible for Writing – review & editing. S. Naganathan contributed to Investigation, Visualization. L. Rajendran contributed to Writing – review & editing, Supervision, Formal analysis. M. Izadi was responsible for Investigation, Validation, Formal Analysis. The manuscript was written through the contribution of all authors. All authors discussed the results, reviewed, and approved the final version of the manuscript.

Acknowledgments

We sincerely thank the reviewers for their insightful and constructive comments, which were invaluable in improving the quality and clarity of this manuscript. Their suggestions greatly helped refine the analysis, enhance interpretation, and strengthen the overall presentation of our study.

Conflict of Interest

The authors declared that there are no conflicts of interest pertaining to the publishing of this article.

Funding

The authors received no financial support for the research, authorship, and publication of this article.

Data Availability Statements

The datasets generated and/or analyzed during the current study are available from the corresponding author on reasonable request.

References

[1] Goodenough, J.B., Electrochemical energy storage in a sustainable modern society, *Energy & Environmental Science*, 7, 2014, 14–18.
[2] Ho, D.P., Ngo, H.H., Guo, W., A mini review on renewable sources for biofuel, *Bioresource Technology*, 169, 2014, 742–749.
[3] Gamella, M., Koushanpour, A., Katz, E., Biofuel cells activation of micro- and macro-electronic devices, *Bioelectrochemistry*, 119, 2018, 33–42.
[4] Nasar, A., Perveen, R., Applications of enzymatic biofuel cells in bioelectronic devices – A review, *International Journal of Hydrogen Energy*, 44, 2019, 15287–15312.
[5] Leech, D., Kavanagh, P., Schuhmann, W., Enzymatic fuel cells: recent progress, *Electrochimica Acta*, 84, 2012, 223–234.
[6] Rajendran, L., Kirthiga, M., Laborda, E., Mathematical modeling of nonlinear reaction diffusion process in enzymatic biofuel cells, *Current Opinion in Electrochemistry*, 1, 2017, 121–132.
[7] Rasmussen, M., Abdellaoui, S., Minteer, S.D., Enzymatic biofuel cells: 30 years of critical advancements, *Biosensors & Bioelectronics*, 76, 2016, 91–102.
[8] Matsumoto, R., Kano, K.T., Ikeda, T., Theory of steady state catalytic current of mediated bioelectrocatalysis, *Journal of Electroanalytical Chemistry*, 535, 2002, 37–40.
[9] Tamaki, T., Ito, T., Yamaguchi, T., Immobilization of hydroquinone through a spacer to polymer grafted on carbon black for a high surface area biofuel cell electrode, *The Journal of Physical Chemistry B*, 111, 2007, 10312–10319.
[10] Tamaki, T., Ito, T., Yamaguchi, T. Modelling of reaction and diffusion processes in a high surface area biofuel cell electrode made of redox polymer grafted carbon, *Fuel Cells*, 9, 2009, 37–43.
[11] Barton, S.C., Kim, H.H., Binyamin, G., Zhang, Y.C., Heller, A., The "Wired" laccase cathode: high current density electroreduction of O_2 to water at +0.7 V (NHE) at pH 5, *Journal of the American Chemical Society*, 123, 2001, 5802–5803.
[12] Davis, F., Higson, S.P.J., Biofuel cells—Recent advances and applications, *Biosensors & Bioelectronics*, 22, 2007, 1224–1235.
[13] Gu, C., Zhang, L., Hou, T., Zhu, D., Li, F., Gai, P., Unveiling the glucose oxidase-like and catalase-like activities of highly conjugated 3,4,9,10-perylenetetracarboxylic dianhydride for boosting biofuel cells, *Advanced Functional Materials*, 34, 2024, e202400617.
[14] Gu, C., Zhang, L., Hou, T., Wang, Q., Li, F., Gai, P., Laser-induced nanozyme biofuel cell-based self-powered patch for accelerating diabetic wound healing with real-time monitoring, *Advanced Functional Materials*, 35, 2025, 23106.
[15] Gu, C., Bai, L., Pu, L., Gai, P., Li, F., Highly sensitive and stable self-powered biosensing for exosomes based on dual metal-organic frameworks nanocarriers, *Biosensors & Bioelectronics*, 176, 2021, 112907.
[16] Song, S., Li, N., Bai, L., Gai, P., Li, F., Photo-assisted robust anti-interference self-powered biosensing of microRNA based on Pt–S bonds and the inorganic–organic hybridization strategy, *Analytical Chemistry*, 94, 2022, 1654–1660.
[17] Bartlett, P.N., Pratt, K.F.E., Modelling of processes in enzyme electrodes, *Biosensors & Bioelectronics*, 8, 1993, 451–462.
[18] Bartlett, P.N., Pratt, K.F.E., A study of the kinetics of the reaction between ferrocene monocarboxylic acid and glucose oxidase using the rotating disc electrode, *Journal of Electroanalytical Chemistry*, 397, 1995, 53–60.
[19] Kano, K., Ikeda, T., Fundamentals and practices of mediated bioelectrocatalysis, *Analytical Sciences*, 16, 2000, 1013–1021.
[20] Yokoyama, K., Kayanuma, Y., Cyclic voltammetric simulation for electrochemically mediated enzyme reaction and determination of enzyme kinetic constants, *Analytical Chemistry*, 70, 1998, 3368–3376.
[21] Barton, S.C., Oxygen transport in composite mediated biocathodes, *Electrochimica Acta*, 50, 2005, 2145–2153.
[22] Wen, H., Nallathambi, V., Chakraborty, D., Barton, S.C., Carbon fiber microelectrodes modified with carbon nanotubes as a new support for immobilization of glucose oxidase, *Microchimica Acta*, 175, 2011, 283–289.
[23] Wen, H., Bambhania, H.M., Barton, S.C., Carbon nanotube modified biocatalytic microelectrodes with multiscale porosity, *Journal of Applied Electrochemistry*, 42, 2012, 145–151.
[24] Osman, M.H., Shah, A.A., Walsh, F.C., Recent progress and continuing challenges in bio fuel cells. Part I: enzymatic cells, *Biosensors & Bioelectronics*, 26, 2011, 3087–3102.
[25] Osman, M.H., Shah, A.A., Walsh, F.C., Recent progress and continuing challenges in bio fuel cells. Part II: microbial, *Biosensors & Bioelectronics*, 26, 2010, 953–963.
[26] Kar, P., Wen, H., Li, H., Minteer, S.D., Calabrese Barton, S.C., Simulation of multistep enzyme catalyzed methanol oxidation in biofuel cells, *Journal of the Electrochemical Society*, 158, 2011, B580.
[27] Rasi, M., Rajendran, L., Sangaranarayanan, M.V., Enzyme catalyzed oxygen reduction reaction in biofuel cells: analytical expressions for chronoamperometric current densities, *Journal of the Electrochemical Society*, 162, 2015, H671–H680.
[28] de Oliveira, D.S.B.L., de Sousa Junior, R., Reaction kinetics-based modeling and parameter sensitivity analysis of direct ethanol fuel cells, *Energies*, 15, 2022, 9143.

[29] Padierna Vanegas, D., Acosta Pavas, J.C., Granados García, L.M., Botero Castro, H.A., Modeling based identifiability and parametric estimation of an enzymatic hydrolysis process of amylaceous materials, *ACS Omega*, 7, 2022, 14544–14555.
[30] Hu, D., Su, Q., Gao, Y., Zhang, J., Wang, L., Zhu, J., Photo nanozyme coupling catalyzes glucose oxidation for high performance enzymatic biofuel cells, *Journal of Materials Chemistry A*, 12, 2024, 25784.
[31] Rizwan, S.M., Sachdeva, K., Al Balushi, N., Al Rashdi, S., Taj, S.Z., Reliability and sensitivity analysis of membrane biofilm fuel cell, *International Journal of Engineering Trends and Technology*, 71, 2023, 73–80.
[32] Saravanakumar, K., Rajendran, L., Sangaranarayanan, M.V., Current–potential response and concentration profiles of redox polymer mediated enzyme catalysis in biofuel cells – estimation of Michaelis–Menten constants, *Chemical Physics Letters*, 621, 2015, 117–123.
[33] Saravanakumar, K., Ganesan, S.P., Rajendran, L., Theoretical analysis of reaction and diffusion processes in a biofuel cell electrode, *Fuel Cells*, 15, 2016, 523–536.
[34] Salomi, R.J., Rajendran, L., Cyclic voltammetric response of homogeneous catalysis of electrochemical reactions: Part 1. A theoretical and numerical approach for EE'C scheme, *Journal of Electroanalytical Chemistry*, 918, 2022, 116429.
[35] Manimegalai, B., Rajendran, L., Cyclic voltammetric response of homogeneous catalysis of electrochemical reactions. Part 3: A theoretical and numerical approach for one electron two step reaction scheme, *Journal of Electroanalytical Chemistry*, 922, 2022, 116706.
[36] Nalini, R., Meena, A., Rajendran, L., Izadi, M., A nonlinear mathematical analysis of nanoparticle's velocity, temperature and concentration in magnetohydrodynamic convective flow, *Partial Differential Equations in Applied Mathematics*, 14, 2025, 101193.
[37] Yamuna, B., Meena, A., Rajendran, L., Izadi, M., An analysis of upper convected Maxwell nanofluid flow over a stretching surface: theoretical and numerical approaches, *Partial Differential Equations in Applied Mathematics*, 14, 2025, 101203.

ORCID iD

R. Rajalakshmi https://orcid.org/0009-0004-4433-9644
A. Marimuthu https://orcid.org/0009-0004-4559-3089
S. Naganathan https://orcid.org/0009-0006-9949-6924
L. Rajendran https://orcid.org/0000-0002-2003-4553
M. Izadi https://orcid.org/0000-0002-6116-4928

How to cite this article: Rajalakshmi R., Marimuthu A., Naganathan S., Rajendran L., Izadi M. Mathematical Modeling and Sensitivity Analysis of Enzymatic Biofuel Cells with Various Electrode Geometries, *J. Appl. Comput. Mech.*, xx(x), 2025, 1–13. https://doi.org/10.22055/jacm.2025.48646.5391